Check for updates

Adsorption of arsenic from aqueous solution using a zero-valent iron material modified by the ionic liquid [Hmim]SbF$_6$

Fenghui Wu, [iD] [ab] Chenyang Zhao, [ab] Guangfei Qu,*[ab] Zhoupeng Yan,[ab] Yingda Zeng,[ab] Bangjin Chen,[ab] Yinghui Hu,[ab] Wei Ji,[ab] Yingli Li[ab] and Huimin Tang[ab]

The environmental and health impacts caused by arsenic (As) in wastewater make it necessary to carefully manage As wastes. In the present work, a composite of the ionic liquid [Hmim]SbF$_6$ and nano-iron (H/Fe) was used as an adsorbent to remove As(v) from aqueous solution. To better understand the removal effect of H/Fe on As(v) in aqueous solution, the reaction parameters of pH, reaction temperature, time and H/Fe dosage were systematically analyzed in detail. The results show that H/Fe has significant removal efficiency toward As(v), and that the adsorption of As(v) by 0.5 g H/Fe reaches its maximum adsorption capacity within 2 h. The adsorption of As(v) on H/Fe is a non-linear, time-varying process. The initial adsorption reaction is fast; however, unlike at the beginning, the later reaction involves sustained slow absorption, resulting in a distinct two-phase adsorption characteristic. Redox reaction may be one of the mechanisms responsible for the slow adsorption of As(v) on H/Fe. At the same time, the As(v) removal effect of H/Fe is greatly restricted by the pH. Electrostatic adsorption, adsorption co-precipitation and redox reactions act together on H/Fe in the As(v) removal process. This study provides a basis for further clarifying the adsorption, adsorption rules and mechanism of As(v) on H/Fe and a feasible method for the improvement of As(v) removal efficiency of zero-valent iron materials.

1. Introduction

With the rapid improvement in environmental protection requirements, arsenic contamination has become the main limiting factor for groundwater.[1] According to the statistics of the World Health Organization,[2] in addition to the catastrophic arsenic pollution in water in Bangladesh and India's Bangladesh region, the United States, Mexico, Chile and other countries still have high concentrations of arsenic in water.[3–5] Long-term exposure to low-dose local arsenic contamination has become one of the most prominent environmental problems domestically and abroad;[6] thus, the international standards for drinking water of arsenic have become stricter.[7]

Current treatment technologies for arsenic-containing water mainly include precipitation, adsorption, ion exchange, neutralization oxidation, ion flotation, electro-flocculation, extraction, membrane separation and biological method, among others.[8–12] Among them, due to its advantages of simplicity, low cost and environmental friendliness, adsorption is the most commonly used method to remove arsenic from

wastewater. Various types of adsorbents have been discussed. Adsorbents usually have very small particle sizes and are easily dispersed in solution. Several absorbents, such as activated carbon, biological adsorbents, mineral adsorbents and graphene, are currently available and have been used in other research. Among them, activated carbon and graphene are the two most commonly used adsorbents;[13,14] however, they have high production costs, which reduces the possibility of their being put into actual production. In particular, their preparation conditions are rather extreme.

Common problems with conventional treatment methods are high cost, the generation of a large amount of waste, and difficulty of separating the adsorbent material from the water.[15] With the development of modern technology, in the past few years, nano-materials have arisen as a new type of adsorbent for application in wastewater treatment,[16,17] but due to their special characteristics, such as the small size of nano-particles, they still present the problem of being difficult to recover from water.[18–20] On these bases, our work provides an alternative method for the efficient adsorption of arsenic. By using magnetic nano-materials,[21,22] easy recycling and reuse can be achieved, environmental pollution can be reduced, and the utilization rate of the nano-adsorbents can be improved. Thus, this approach shows great promise for a wide range of applications in the challenging removal of arsenic of wastewater for environmental protection. Nano-zero-valent iron (NZVI) is

Faculty of Environmental Science and Engineering, Kunming University of Science and Technology, Kunming 650500, Yunnan, People's Republic of China. E-mail: qgflab@sina.com

National Regional Engineering Research Center-NCW, Kunming 650500, Yunnan, People's Republic of China

a chemical reductant with strong chemical reducibility.[23] Due to its unique surface effect and small size effect, it has superior adsorption performance and high reducing activity. NZVI has been reported as a successful remediation agent for environmental issues, and is extensively used in groundwater and soil remediation.[24,25] The use of zero-valent nanoparticles has arisen as a highly effective method due to their high specific surface area, and developments in the properties of the nano-particles have promoted the application of NZVI in environmental remediation technologies.[26]

In recent years, ionic liquids (ILs) have been considered to be green chemicals and have been regarded as environmentally friendly substitutes for toxic organic solvents. ILs have the characteristics of non-volatility, water-stability, reusability, low melting points and environment friendly solubility;[27] thus, the study of the ionic-liquid-based extraction of various metal ions, copper, nano-plastics and radioactive metals,[28,29] among other contaminants, has become a research hot spot. Many types of ILs, such as imidazolium-based and pyridinium-based ILs, are water-stable. Therefore, the toxicity of these types of ILs, especially imidazolium-based ILs, has a limited effect in the water phase.[30] Furthermore, imidazolium-based ILs are non-volatile, especially compared to other commonly used organic chemicals, *i.e.*, ammonia and phenol. Imidazolium-based ILs do not evaporate into the atmosphere, and thus do not contribute to air pollution, such as smog formation, ozone depletion and global climate change. Most importantly, imidazolium-based ILs will not lead to human inhalation exposure or injury due to fires and explosions.[30–33] However, the use of ionic liquids as adsorbents for the removal of arsenic is limited by some challenges. Several disadvantages, such as the need for a large IL dosage, and the high price, high viscosity, difficult separation after use and slow reaction processes of ILs greatly limit their use in large-scale industrial applications.[34] Therefore, in order to avoid the disadvantages of ionic liquids and enable them to be applied on a large scale, porous adsorbents have been used as carriers onto which the ionic liquid can be loaded.[35,36] The novel adsorbents prepared in this way not only exhibit the advantages of both the ionic liquid and the adsorbent, but also avoid the problems associated with ionic liquids. Therefore, they not only can reduce the amount of ionic liquid added, thereby reducing the cost, but also facilitate the expansion of the surface area, promote the reaction process, and greatly extend the practical use of ionic liquids.[37–39]

In many studies, surfactant-based modified adsorbents have been found to be an appropriate choice, and modified adsorbents have been shown to play a very big role in enhancing the adsorption efficiency of various materials.[40] On this theoretical basis, in our present study, the ionic liquid [Hmim]SbF$_6$ was chosen for modifying nano-zero-valent iron particles because of its ability to be grafted onto NZVI. As a result, the number of free radical functional groups on the zero-valent nano-iron increased, and both the stability of the zero-valent nano-iron and its adsorption capacity toward the pollutant arsenic were improved. The [Hmim]SbF$_6$–nano-iron (H/Fe) composite adsorbent was prepared *via* a physical impregnation method,

and its arsenic removal ability and mechanism in aqueous solution were investigated.

2. Experimental

2.1 Materials and instrumentation

NZVI powder (polycrystalline nano-iron with a face-centered cubic structure, purity 99%) with a claimed average particle size of <50 nm was purchased from Tianjin Damao Chemical Reagent Factory (China). An arsenic standard solution with a concentration of 1000 mg L^{-1} was purchased from Xiya Chemical Reagent Factory, and mainly contained total arsenic, which includes As(V) and a small amount of As(III). 1-Methylimidazole and *N*-hexane chloride were bought from Lanzhou Institute of Chemicals (China), ethyl acetate was obtained Jinan Haili Chemical Co., Ltd. (China), and antimony pentafluoride was purchased from Tianjin Special Gas Company (China). All chemical reagents used in the experiment were of analytical purity (AR), and deionized water was used as a solvent.

The instruments used in the experiments were an AFS-933 atomic fluorescence spectrometer (Beijing Jitian Instrument Co., Ltd., China), ZSX100e X-ray fluorescence spectrometer (Tianjin Gongdong Sci. & Tech. Co., Ltd., China), TTRIII X-ray diffractometer (Dandong Tongda Technology Co., Ltd., China), AXIS-ULTRA DLD-600W X-ray photoelectron spectrometer (Shimadzu Enterprise Management (China) Co., Ltd), rotary distillation apparatus and CS101-1AB electrothermal constant temperature blast drying oven and hydride generator (Shanghai Jiecheng Experimental Instrument Co., Ltd., China).

2.2 Preparation of [Hmim]SbF$_6$

2.2.1 Synthesis of [Hmim]Cl. 1-Methylimidazole and *n*-hexane chloride were mixed in a 1 : 1.2 molar ratio in a three-port flask with a reflux device. The reaction temperature was controlled at 70 °C using a heat-collecting constant-temperature heating magnetic stirrer. The reaction was carried out under magnetic stirring and stopped after 24 h. The crude product was washed with ethyl acetate 3–4 times to remove the unreacted raw materials and then dried in a rotary evaporator at 80 °C. Finally, [Hmim]Cl was obtained as a colorless transparent viscous liquid after vacuum drying at 80 °C for 24 h.

2.2.2 Synthesis of [Hmim]SbF$_6$. [Hmim]Cl was synthesized *via* the two-step method, and [Hmim]SbF$_6$ was then obtained by ion exchange. [Hmim]Cl and HSbF$_6$ were mixed in a 1 : 1.2 ratio in a three-port flask with a reflux device. The same volume of distilled water was added. The reaction temperature was controlled at 80 °C by a heat-collecting constant-temperature magnetic stirrer. The reaction was carried out under magnetic stirring and stopped after 24 h. The reaction mixture was then left to stand to allow it to stratify. The upper layer of distilled water was poured out and washed repeatedly with the same volume of steam feed water to remove unreacted HSbF$_6$. Finally, the washed ionic liquid was placed in an empty drying oven to dry it and remove the water, after which the colorless transparent viscous liquid [Hmim]SbF$_6$ was obtained.

2.3 Preparation and characterization of materials

The ionic liquid was loaded onto the nano-materials by a physical method. First, 1.0 g of the nano-iron material was immersed in 1.3 g of [Hmim]SbF$_6$ in the same beaker at 35 °C for 24 hours. The solution was filtered while hot and washed repeatedly before being dried in an oven for later use.

Surface morphology studies were performed using scanning electron microscopy (SEM, FEI Quanta-200) images and high-resolution transmission electron microscopy (HR-TEM, JEM-2100). The specific surface area and pore volume were evaluated using a Brunauer–Emmett–Teller (BET, ASAP 2000, Micromeritics, USA) nitrogen adsorption–desorption isotherm. The surface composition was examined *via* X-ray photoelectron spectroscopy (XPS) using a VG ESCALAB Mg Ka X-ray source device, and the binding energy was calibrated using the C1s peak at 284.6 eV.

2.4 Adsorption experiments

The total arsenic concentration was 1.00 mg L^{-1}, and a known amount of H/Fe was added. According to the single factor variable method, the reaction temperature, reaction time, solution pH and dosage of the adsorbent were used as variables to investigate the effect of arsenic removal and determine the optimal adsorption conditions. The supernatant was then aspirated, and the concentration of total arsenic remaining was determined by atomic fluorescence spectrometry after the pre-treatment. The calculation formulae for the adsorption amount and adsorption efficiency are shown below:

$$q_e = \frac{C_0 - C_e}{m} \times V \tag{1}$$

$$\eta = \frac{C_0 - C_e}{C_0} \times 100\% \tag{2}$$

where q_e is the adsorption amount (mg g^{-1}) at the adsorption equilibrium, C_0 and C_e are the initial concentration of the solution and the concentration at adsorption equilibrium (mg L^{-1}), V is the volume of the solution (L), m is the dosage of the adsorbent (g), and η is the removal rate (%).

3. Results

3.1 Sample characterization and analysis

3.1.1 SEM, BET and EDS analysis. SEM images of the ionic-liquid-loaded nanomaterials are shown in Fig. 1a and b, which depict the microstructure of NVZI and H/Fe respectively. Fig. 1c is the adsorption isotherm and pore size distribution of NZVI before and after ionic liquid loading, and Fig. 1d is the EDS result for the ionic-liquid-loaded NZVI. As can be seen from the SEM images (Fig. 1a and b), an ionic liquid film is formed on the H/Fe surface. From Fig. 1d, it can be seen that the H/Fe surface has C, N, O, F, and Sb peaks in addition to Fe peaks, which implied that the ionic liquid was grafted onto iron. The pollutant arsenic reacts directly with the iron surface groups, indicating the impregnation method does immobilize the ionic liquid [Hmim]SbF$_6$ on the surface of the modified nano-iron.
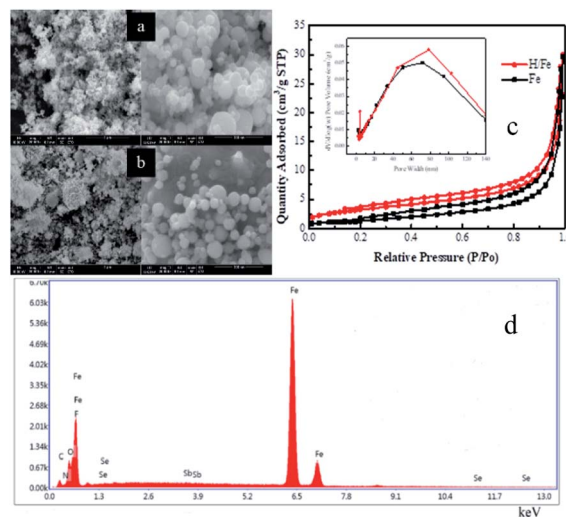

Fig. 1 SEM photos of the ionic-liquid-loaded nanomaterials: (a) NZVI; (b) H/Fe. (c) Adsorption isotherm and pore size distribution of NZVI before and after ionic liquid loading. (d) EDS results for ionic-liquid-loaded NZVI.

BET analysis indicates that the specific surface area and pore volume increase after ionic liquid loading. It can be seen from Fig. 1c that the specific surface area of the nano-iron increased by 16.11% and the cumulative pore volume increased by 27% after loading the ionic liquid. This shows that the ionic liquid is supported on the surface of the nano-iron, increasing the surface roughness and forming part of the pores, which in turn enhances the possibility of N$_2$ coming into contact with the internal pores of the material during the adsorption process and finally results in an increase in specific surface area. In addition, the average pore size also increased after modification. From the pore size distribution map in Fig. 1c and the average pore diameter shown in Table 1, it can be seen that the mesopores and macropores on the nano-iron surface increased after the ionic-liquid loading, with the average pore size increasing by approximately 15%. This indicates that the ionic liquid on the surface of the material also contributes to the porosity and specific surface area.

3.1.2 XPS analysis. The chemical composition of fresh and used H/Fe was analysed using an X-ray photoelectron spectrometer with a monochromated Al K$_\alpha$ source at a power of 450 W. The XPS analysis of the fresh and used H/Fe over the O 1s, N 1s, and C 1s spectral regions are shown in Fig. 2a, b and c, respectively. The figure shows that the O 1s XPS spectrum of ionic-liquid-loaded nano-iron can be deconvoluted into three peaks at 529.8, 531.1 and 534.3 eV, respectively. The first peak is

Table 1 Materials structure parameters before and after IL-loading

Material	S_{BET} (m^2 g^{-1})	D (nm)	V_{total} (cm^3 g^{-1})
Fe	11.86	18.60	0.045
HSbF–Fe	13.77	21.44	0.057

Fig. 2 XPS spectra of fresh and used H/Fe over the (a) O 1s, (b) N 1s, and (c) C 1s spectral regions.

Fig. 3 Effect of the reaction temperature on the adsorption of As.

attributed to lattice oxygen (expressed as O_α), the second peak is attributed to chemisorbed oxygen (expressed as O_β) and the third peak corresponds to carbonyl oxygen (–CO–, expressed as O_γ). Among them, the functional group is attributed to the partial oxidation and activation of nano-iron during the calcination process, and O_β is the most active oxygen during the oxidation reaction.[41] Table 2 shows the change in the percentage of O 1s for the ionic-liquid-loaded nano-iron before and after the reaction. After the reaction, O_γ disappears completely, and O_α and O_β increase, indicating that all the carbonyl oxygen is consumed in the reaction, resulting in more chemisorbed or hydroxyl oxygen and NO_3^-. Fig. 2c shows the spectrum of Fe 2p. The peaks at 710.0 and 710.8 eV were attributed to Fe^{2+} cations, and the peaks at 713 and 719 eV in the center belong to Fe^{3+} cations.[42,43] The percentage of Fe^{2+} ($Fe^{2+}/(Fe^{2+}+Fe^{3+})$) was 20.79% in the unreacted material, and increased to 41.08% after the reaction.[44] The study shows that Fe^{3+} can effectively capture electrons due to its radius (0.69 Å); in addition, the redox performance of the Fe^{2+}/Fe^{3+} combination is higher.[45] Therefore, Fe^{2+} is easily oxidized by H^+ or adsorbed O_2 to Fe^{3+}.[46]

3.2 Effect of the main environmental factors on the adsorption of As(v)

3.2.1 Effect of reaction temperature.
In order to investigate the effects of reaction temperature on the As(v) removal efficiency, adsorption experiments were conducted at six different
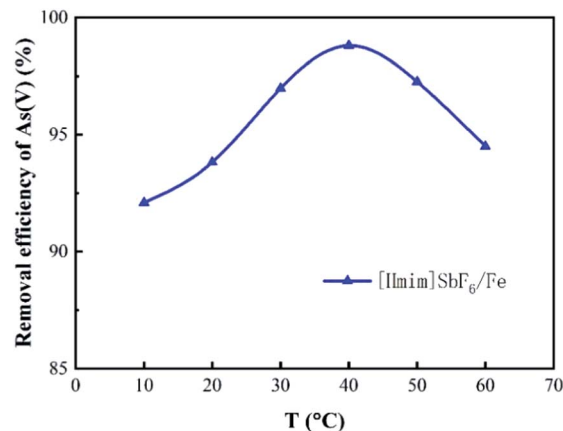
temperatures (10, 20, 30, 40, 50 and 60 °C). In this experiment, 6 0.5 g portions of H/Fe were weighed out, and each was added to 1.0 L of arsenic-containing wastewater with an arsenic concentration of 1 mg L^{-1}. The adsorption time was 12 h. The experimental results showing the influence of the reaction temperature on the total arsenic adsorption by H/Fe are presented in Fig. 3. One regular phenomenon that can be observed is that as the temperature increases, the arsenic removal efficiency of H/Fe increases when the temperatures is below 40 °C. However, as the temperature continues to rise above 40 °C, the arsenic removal efficiency gradually declines. This result implies that when the temperature is low, the combination of the pore structure of the adsorbent and the arsenic ion is not active, and the non-covalent bond between them increases with increasing temperature. Furthermore, it also indicates that the H/Fe surface has more iron oxide at 40 °C and the iron is more reactive with arsenate ions to form precipitates. When the temperature exceeds 40 °C, the arsenic ions in the liquid phase move more frequently, which is not conducive to adsorption, and even some arsenic begins to be re-solvated. Therefore, 40 °C was selected as the optimum experimental adsorption condition for H/Fe.

3.2.2 Effect of reaction time.
To determine the effect of reaction time on the As(v)removal efficiency, the adsorption experiment was carried out at 40 °C for 24 h. In this experiment, 0.5 g H/Fe was weighed and added to 1.0 L of arsenic-containing wastewater with an arsenic concentration of 1.00 mg L^{-1}. The relationship between the adsorption efficiency and the reaction time is shown in Fig. 4. It can be seen from the figure that the adsorption of arsenic in water can be divided into two stages: a rapid adsorption stage and slow adsorption. The rapid adsorption phase of H/Fe is observed during the first 90 min of adsorption. During this period of time, the arsenic removal efficiency is approximately 99%, and the arsenic removal efficiency reaches adsorption equilibrium at 99.5% in the slow adsorption phase. Considering the adsorption effect and the experimental progress of the experiment, we selected 2 h as the adsorption time condition for the subsequent experiments.

Table 2 Surface O and C atom percentages on the ionic-liquid-loaded nanomaterial

Nano-material	O (%)			C (%)		
	O_α	O_β	O_γ	C_α	C_β	C_γ
Fresh H/Fe	19.56	33.40	47.07	28.79	30.36	40.85
Used H/Fe	36.35	63.65	—	50.07	38.09	11.84

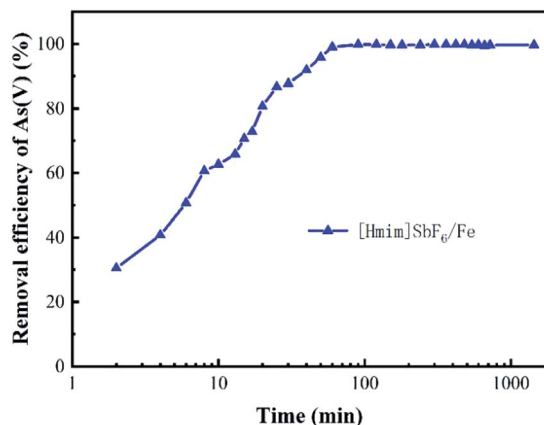Fig. 4 Influence of reaction time on the arsenic removal rate.

Fig. 6 Influence of dosage on the arsenic removal rate.

3.2.3   Effect of solution pH. The effect of the solution pH on the As(v) removal efficiency was conducted at pH values of 2, 4, 6, 8, and 10, respectively. In the experiment, six 0.5 g portions of H/Fe were weighed out, and each was added to 1.0 L of arsenic-containing wastewater with an arsenic concentration of 1.00 mg L^{-1}. The adsorption experiment was carried out at 40 °C for 2 h, and the relationship between the adsorption effect of H/Fe and the pH of the solution is shown in Fig. 5. The figure suggests that the arsenic removal efficiency of the H/Fe pair is highest when the pH is 6, but after pH exceeds 6, the arsenic removal efficiency drops dramatically, and when the pH is 12, it reaches 43%. This is because the material easily precipitates when OH$^-$ forms iron hydroxide and ferrous hydroxide under alkaline conditions. Although the newly formed substance adsorbs some arsenic ions by coprecipitation, it also adheres to the surface of the material to passivate it, reducing the arsenic removal efficiency. When the pH is low, the acidic solution is more favourable for the production of Fe^{2+} on the surface of the adsorbent. The Fe^{2+} can be rapidly oxidized to Fe^{3+}, and the arsenate precipitate is formed by the redox reaction and the arsenate ion to improve the arsenic removal efficiency.

3.2.4   Effect of H/Fe dosage. The effect of the H/Fe dosage on the removal efficiency of As(v) was investigated in this experiment. 0.05 g, 0.1 g, 0.3 g, 0.5 g, 0.7 g, or 1.0 g H/Fe were weighed out and added to 1.0 L of arsenic-containing
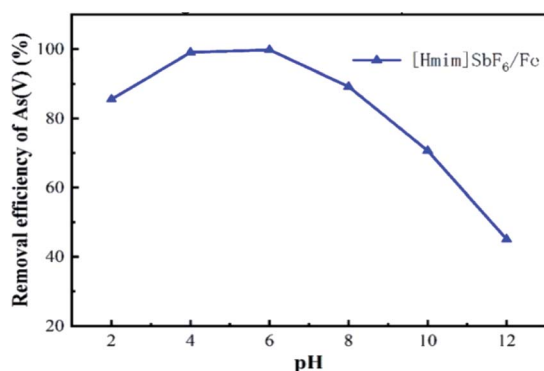
wastewater with an arsenic concentration of 1 mg L^{-1} to control the pH of the water sample to 6. The adsorption experiment was carried out at 40 °C for 2 h, and the relationship between the adsorption effect of H/Fe and the dosage is shown in Fig. 6. It can be seen from the figure that H/Fe has a good removal efficiency toward arsenic, and that a high removal rate can be achieved using a very low dosage. The arsenic removal performance increases with increasing H/Fe dosage. When the amount of H/Fe reaches 0.5 g L^{-1}, the maximum adsorption is achieved. As the dose of the adsorbent is increased, the number of adsorption sites for arsenic on the adsorbent and the removal efficiency of arsenic increase. At the same time, the amounts of Fe^{2+}, Fe^{3+} and Fe(OH)$_3$ on H/Fe also increase, that is, the formation of FeAsO$_4$ precipitates and coprecipitates to remove arsenic becomes easier. In addition, the increase in ionic liquid causes the positive charge on the surface of the material to increase and the viscosity increases, thereby leading to the adsorption of more arsenic anions.

3.2.5   Adsorption equation. Six portions of 0.5 g H/Fe were weighed and added to 1.0 L of arsenic-containing wastewater, for the assessment of arsenic concentration on the removal efficiency, different initial concentrations of arsenic (C$_0$), namely, 0.5, 1, 1.5, 2, 2.5, 3, and 5, 9 mg L^{-1} were investigated,

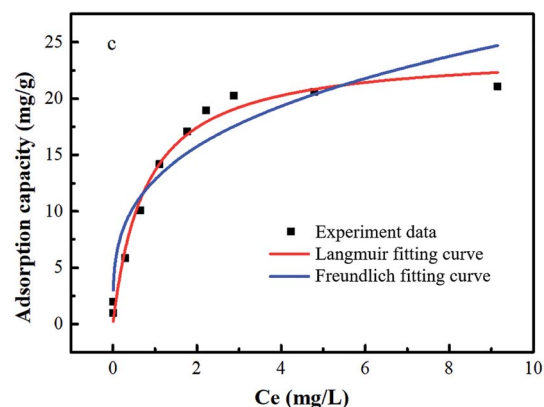Fig. 5 Influence of pH on arsenic removal efficiency.

Fig. 7 Fitting of the H/Fe adsorption isotherm by the Langmuir and Freundlich equations.

the reaction pH was 6, and the adsorption experiment was carried out at 40 °C for 2 h. The equilibrium concentration was then measured, and the equilibrium adsorption amount was calculated. The data were fitted using the Langmuir and Freundlich isotherm adsorption equations. The results are shown in Fig. 7, and the parameters are shown in Table 3.

Table 3 suggests that the fitting degree of the Freundlich isotherm equation ($R^2 = 0.9818$) for the H/Fe adsorption arsenic isotherm is greater than that of the Langmuir isotherm equation ($R^2 = 0.9016$), and the data is thus better described by the Freundlich equation. The adsorption of arsenic on H/thus mainly involves chemical adsorption of multi-molecular layers.

4. Discussion

This experiment showed that H/Fe is very effective in adsorbing the pollutant arsenic. The adsorption process may involve not only simple physical adsorption, but also chemical adsorption and coprecipitation processes. When the reaction begins, the NZVI surface not covered by the ionic liquid is gradually oxidized during the adsorption process. At the same time, a small amount of As(v) is reduced to As(iii). Additionally, oxides or hydroxides may also have an effect on the adsorption of arsenic ions.[28,37,47] The H/Fe removed As(v) by two main routes: adsorption by the ionic liquid or adsorption by the NZVI. These adsorption mechanisms are described below:

4.1 Ionic liquid removal of arsenic

The ionic liquid supported by the adsorbent contains electron donor atoms such as nitrogen and oxygen, and the lone pair electrons provided can cooperate with AsO_4^{3-} and AsO_3^{3-} to produce stable complex products, thereby achieving the purpose of removing arsenic. Nevertheless, electro-adsorption and ion exchange reactions may occur at the same time. The ionic liquid supported on the surface of the adsorbent consists of anions and cations. The cations electrostatically adsorb the AsO_4^{3-} and AsO_3^{3-} anions in the aqueous solution, which simultaneously displace the ionic liquid anions.

4.2 NZVI removal of arsenic

Fig. 8 presents the relationship between the zeta potential and pH. The figure shows that the zeta potential of H/Fe is 7.03, and suggests that when the pH value is below 7.03, the surface is positively charged, which promotes electrostatic adsorption. That is, H/Fe has the best adsorption performance for arsenic under weakly acidic conditions (its large specific surface area and abundant pore structure are also beneficial for adsorbing arsenic in water).
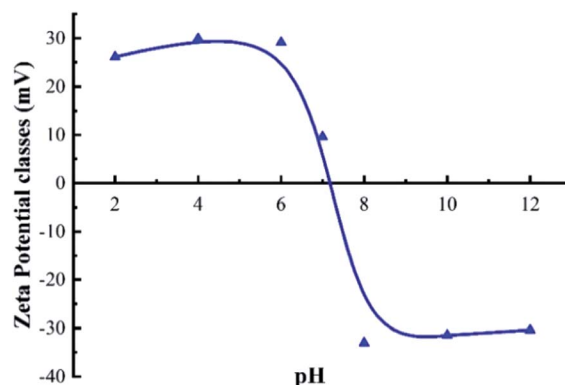

Fig. 8 Zeta potential of H/Fe.

When the pH value is below 7, the H^+ in solution is conducive to the production of more Fe^{2+} on the surface of the adsorbent. This Fe^{2+} can be rapidly oxidized to Fe^{3+}, and the arsenate precipitate is formed by the redox reaction and the arsenate ion to improve the arsenic removal effect. Furthermore, As(iii) exists as arsenic acid, and $H_2AsO_3^-$ appears only after the pH exceeds 7. However, the formation of ferrous arsenate is very difficult, so only the formation of ferric arsenate is observed:

$$Fe^{3+} + AsO_4^{3-} = FeAsO_4\downarrow \tag{3}$$

When pH exceeds 7, the following reaction between AsO_4^{3-} and $Fe(OH)_3$ in solution would proceed:

$$Fe(OH)_3 + AsO_4^{3-} = FeAsO_4\downarrow + 3OH^- \tag{4}$$

In addition, $Fe(OH)_3$ coprecipitates with As(v) to remove part of As(v). However, when the pH is too low or too high, the solubility of $FeAsO_4$ increases, thereby releasing arsenic, which leads to an increase in the concentration of iron and arsenic ions in the solution system and reduces the arsenic removal efficiency.

The adsorption stability of arsenic adsorbed on the surface of NZVI is mainly caused by precipitation and adsorption. The adsorption includes non-specific adsorption (physical adsorption) and specific adsorption (chemical adsorption). Furthermore, the pH can affect not only the surface charge of the particles, but also the formation of ferric hydroxide colloids, which in turn affects both non-specific and specific adsorption. Oxygen oxidizes the arsenic ions in the solid phase into arsenate ions, which react with the loaded ferric ions. Ferric hydroxide generated ferric arsenate, adsorbed arsenate, arsenate, etc., replace the ferric hydroxide surface polynuclear complex ion –OH and –OH$_2$-based ligands generated by the coordination of the amorphous state ferric arsenate precipitate.

5. Conclusion

The application of H/Fe for the adsorption of arsenic from polluted water has been assessed experimentally, and the results indicate that a rapid adsorption process and a slow

Table 3 H/Fe adsorption isotherm parameters

Sample	Langmuir parameters			Freundlich parameters		
	Q_m (mg g^{-1})	b (mg L^{-1})	R^2	K_f (mg g^{-1})	n	R^2
HSb–Fe	12.81	0.298	0.9016	24.23	0.781	0.9818

adsorption process occur. This may suggest two stages, namely, electrostatic attraction and surface complexation or ion exchange between the adsorbate and adsorbent.[48,49] Various operating parameters, including the reaction temperature, reaction time, solution pH and dosage of the adsorbent have been systematically evaluated. It was found that when arsenic is adsorbed at low pH, the surface of the adsorbent is positively charged, which generates electrostatic attraction with negatively charged arsenic anions such as $H_2AsO_3^-$, $HAsO_4^{2-}$ and AsO_4^{3-} in the solution, thus causing a strong arsenic removal effect. A significant decrease of As(v) adsorption occurs when the pH is increased because the positive charge on the surface of H/Fe decreases and the interaction between H/Fe and As(v) becomes smaller and repulsive. However, As(III) will cause the H/Fe surface to be more complicated in neutral solution, leading to an increase in adsorption. The immobilization of the ionic liquid, which has the characteristics of high viscosity, hydrogen bonding ability, and charge, on the nano-iron remarkably improved its removal efficiency. The cations in the ionic liquid adsorb on the surface and inside of the nano-iron to form a monolayer. In addition, as the solid-state ratio increases, the cations in the ionic liquid form a bilayer on the material due to the micelles, which can reverse the charge of the material. Therefore, it is positively charged, which is favourable for the adsorption of arsenic. The imidazole structure and various functional groups of the ionic liquid can also coordinate with the arsenic-containing ions. As a result, the removal efficiency of arsenic by H/Fe becomes high, mainly due to the chemical adsorption of a multi-molecular layer.

Additionally, the ionic liquid causes a significant increase in the effective adsorption sites of the nano-iron. The arsenic in the wastewater combines with the effective adsorption sites on H/Fe and is fixed on the surface of the adsorbent material, leading to promising adsorption efficiency. The zeta potential of H/Fe is 7.03. Thus, when pH is below 7.03, the positively charged surface promotes electrostatic adsorption. As a result, H/Fe has the best arsenic adsorption performance under weakly acidic conditions and there are more iron ions at lower pH, resulting in more iron arsenate precipitation.

Conflicts of interest

The authors declared that they have no conflicts of interest to this work. We declare that we do not have any commercial or associative interest that represents a conflict of interest in connection with the work submitted.

Acknowledgements

References

1 J. Podgorski and M. Berg, Global threat of arsenic in groundwater, *Science*, 2020, **368**, 845–848.

2 T. C. Egbosiuba, A. S. Abdulkareem, A. S. Kovo, E. A. Afolabi, J. O. Tijani and W. D. Roos, Enhanced adsorption of As(V) and Mn(VII) from industrial wastewater using multi-walled carbon nanotubes and carboxylated multi-walled carbon nanotubes, *Chemosphere*, 2020, **254**, 230–243.

3 M. C. Teixeira, A. C. Santos, C. S. Fernandes and J. C. Ng, Arsenic contamination assessment in Brazil - Past, present and future concerns: A historical and critical review, *Sci. Total Environ.*, 2020, **730**, 138217.

4 D. Chakraborti, S. K. Singh, M. M. Rahman, R. N. Dutta, S. C. Mukherjee, S. Pati and P. B. Kar, Groundwater Arsenic Contamination in the Ganga River Basin: A Future Health Danger, *Int. J. Environ. Res. Public Health*, 2018, **15**(2), 180.

5 F. M. Yunus, S. Khan, P. Chowdhury, A. H. Milton, S. Hussain and M. Rahman, A Review of Groundwater Arsenic Contamination in Bangladesh: The Millennium Development Goal Era and Beyond, *Int. J. Environ. Res. Public Health*, 2016, **13**(250), 1–18.

6 I. Palma-Lara, M. Martinez-Castillo, J. C. Quintana-Perez, M. G. Arellano-Mendoza, F. Tamay-Cach, O. L. Valenzuela-Limon, E. A. Garcia-Montalvo and A. Hernandez-Zavala, Arsenic exposure: A public health problem leading to several cancers, *Regul. Toxicol. Pharmacol.*, 2020, **110**, 1–35.

7 M. M. El-Bahnasawy, A. E.-H. Mohammad and T. A. Morsy, Arsenic pesticides and environmental pollution: exposure, poisoning, hazards and recommendations, *Journal of the Egyptian Society of Parasitology*, 2013, **43**, 493–508.

8 A. Ahmad, L. Heijnen, L. de Waal, F. Battaglia-Brunet, W. Oorthuizen, B. Pieterse, P. Bhattacharya and A. van der Wal, Mobility and redox transformation of arsenic during treatment of artificially recharged groundwater for drinking water production, *Water Res.*, 2020, **178**, 115826.

9 X. Huang, C. Zhu, Q. Wang and G. Yang, Mechanisms for As(OH)(3) and H3AsO4 adsorption at anhydrous and hydrated surfaces of gibbsite and possibility for anionic As(III) and As(V) formation, *Appl. Surf. Sci.*, 2020, **525**, 146494.

10 M. Kobya, M. S. Oncel, E. Demirbas and M. Celen, Arsenic and boron removal from spring and groundwater samples in boron mining regions of Turkey by electrocoagulation and ion-exchange consecutive processes, *Desalin. Water Treat.*, 2017, **93**, 288–296.

11 E. E. Canas Kurz, V. T. Luong, U. Hellriegel, F. Leidinger, T. L. Luu, J. Bundschuh and J. Hoinkis, Iron-based subsurface arsenic removal (SAR): Results of a long-term pilot-scale test in Vietnam, *Water Res.*, 2020, **181**, 115929.

12 V. T. Luong, E. E. C. Kurz, U. Hellriegel, T. L. Luu, J. Hoinkis and J. Bundschuh, Iron-based subsurface arsenic removal technologies by aeration: A review of the current state and future prospects, *Water Res.*, 2018, **133**, 110–122.

13 V. Kumar, Y.-S. Lee, J.-W. Shin, K.-H. Kim, D. Kukkar and Y. F. Tsang, Potential applications of graphene-based nanomaterials as adsorbent for removal of volatile organic compounds, *Environ. Int.*, 2020, **135**, 105356.

14 G. Skouteris, D. Saroj, P. Melidis, F. I. Hai and S. Ouki, The effect of activated carbon addition on membrane bioreactor processes for wastewater treatment and reclamation - A critical review, *Bioresour. Technol.*, 2015, **185**, 399–410.

15 S. Alka, S. Shahir, N. Ibrahim, M. J. Ndejiko, D.-V. N. Vo and F. A. Manan, Arsenic removal technologies and future trends: A mini review, *J. Cleaner Prod.*, 2021, **278**, 123805.

16 T. K. Das, T. S. Sakthivel, A. Jeyaranjan, S. Seal and A. N. Bezbaruah, Ultra-high arsenic adsorption by graphene oxide iron nanohybrid: Removal mechanisms and potential applications, *Chemosphere*, 2020, **253**, 126702.

17 J. Xiong, D. Zhang, H. Lin and Y. Chen, Amphiprotic cellulose mediated graphene oxide magnetic aerogels for water remediation, *Chem. Eng. J.*, 2020, **400**, 125890.

18 W. H. M. Abdelraheem, M. N. Nadagouda and D. D. Dionysiou, Solar light-assisted remediation of domestic wastewater by NB-TiO2 nanoparticles for potable reuse, *Appl. Catal., B*, 2020, **269**, 118807.

19 Y. Zhang, A. Diehl, A. Lewandowski, K. Gopalakrishnan and T. Baker, Removal efficiency of micro- and nanoplastics (180 nm–125 μm) during drinking water treatment, *Sci. Total Environ.*, 2020, **720**, 137383.

20 V. S. Sousa and M. Ribau Teixeira, Metal-based engineered nanoparticles in the drinking water treatment systems: A critical review, *Sci. Total Environ.*, 2020, **707**, 136077.

21 Z. Wen, J. Lu, Y. Zhang, G. Cheng, S. Huang, J. Chen, R. Xu, Y.-a. Min, Y. Wang and R. Chen, Facile inverse micelle fabrication of magnetic ordered mesoporous iron cerium bimetal oxides with excellent performance for arsenic removal from water, *J. Hazard. Mater.*, 2020, **383**, 121172.

22 M. Shirani, S. Habibollahi and A. Akbari, Centrifuge-less deep eutectic solvent based magnetic nanofluid-linked air-agitated liquid-liquid microextraction coupled with electrothermal atomic absorption spectrometry for simultaneous determination of cadmium, lead, copper, and arsenic in food samples and non-alcoholic beverages, *Food Chem.*, 2019, **281**, 304–311.

23 J. Semerad, N. I. N. Pacheco, A. Grasserova, P. Prochazkova, M. Pivokonsky, L. Pivokonska and T. Cajthaml, In Vitro Study of the Toxicity Mechanisms of Nanoscale Zero-Valent Iron (nZVI) and Released Iron Ions Using Earthworm Cells, *Nanomaterials*, 2020, **10**, 2189.

24 Z.-H. Diao and W. Chu, FeS2 assisted degradation of atrazine by bentonite-supported nZVI coupling with hydrogen peroxide process in water: Performance and mechanism, *Sci. Total Environ.*, 2021, **754**, 11459.

25 D. Summer, P. Schoeftner, B. Wimmer, M. Pastar, T. Kostic, A. Sessitsch, M. H. Gerzabek and T. G. Reichenauer, Synergistic effects of microbial anaerobic dechlorination of perchloroethene and nano zero-valent iron (nZVI) - A lysimeter experiment, *New Biotechnol.*, 2020, **57**, 34–44.

26 J. Fan, X. Chen, Z. Xu, X. Xu, L. Zhao, H. Qiu and X. Cao, One-pot synthesis of nZVI-embedded biochar for remediation of two mining arsenic-contaminated soils: Arsenic immobilization associated with iron transformation, *J. Hazard. Mater.*, 2020, **398**, 121174.

27 I. S. Kurnik, M. A. Noronha, M. C. C. Camara, P. G. Mazzola, A. A. Vicente, J. F. B. Pereira and A. M. Lopes, Separation and purification of curcumin using novel aqueous two-phase micellar systems composed of amphiphilic copolymer and cholinium ionic liquids, *Sep. Purif. Technol.*, 2020, **250**, 113849.

28 Q. Yang, C. H. Lau and Q. Ge, Novel Ionic Grafts That Enhance Arsenic Removal via Forward Osmosis, *ACS Appl. Mater. Interfaces*, 2019, **11**, 17828–17835.

29 R. Elfgen, S. Gehrke and O. Holloczki, Ionic Liquids as Extractants for Nanoplastics, *Chemsuschem*, 2020, **13**(20), 112430.

30 R. J. Bernot, M. A. Brueseke, M. A. Evans-White and G. A. Lamberti, Acute and chronic toxicity of imidazolium-based ionic liquids on Daphnia magna, *Environ. Toxicol. Chem.*, 2005, **24**, 87–92.

31 C.-W. Cho, T. P. T. Pham, Y.-C. Jeon and Y.-S. Yun, Influence of anions on the toxic effects of ionic liquids to a phytoplankton Selenastrum capricornutum, *Green Chem.*, 2008, **10**, 67–72.

32 A. Kumar, M. Bisht and P. Venkatesu, Biocompatibility of ionic liquids towards protein stability: A comprehensive overview on the current understanding and their implications, *Int. J. Biol. Macromol.*, 2017, **96**, 611–651.

33 P. Thi Phuong Thuy, C.-W. Cho and Y.-S. Yun, Environmental fate and toxicity of ionic liquids: A review, *Water Res.*, 2010, **44**, 352–372.

34 N. Nasirpour, M. Mohammadpourfard and S. Z. Heris, Ionic liquids: Promising compounds for sustainable chemical processes and applications, *Chem. Eng. Res. Des.*, 2020, **160**, 264–300.

35 T. J. Szalaty, L. Klapiszewski and T. Jesionowski, Recent developments in modification of lignin using ionic liquids for the fabrication of advanced materials-A review, *J. Mol. Liq.*, 2020, **301**, 112417.

36 J. Rios-Gomez, M. Teresa Garcia-Valverde, A. Inmaculada Lopez-Lorente, C. Toledo-Neira, R. Lucena and S. Cardenas, Polymeric ionic liquid immobilized onto paper as sorptive phase in microextraction, *Anal. Chim. Acta*, 2020, **1094**, 47–56.

37 V. R. Thamke, A. U. Chaudhari, S. R. Tapase, D. Paul and K. M. Kodam, In vitro toxicological evaluation of ionic liquids and development of effective bioremediation process for their removal, *Environ. Pollut.*, 2019, **250**, 567–577.

38 M. Koutinas, M. I. Vasquez, E. Nicolaou, P. Pashali, E. Kyriakou, E. Loizou, A. Papadaki, A. A. Koutinas and L. Vyrides, Biodegradation and toxicity of emerging contaminants: Isolation of an exopolysaccharide-producing Sphingomonas sp. for ionic liquids bioremediation, *J. Hazard. Mater.*, 2019, **365**, 88–96.

39 S. Marullo, C. Rizzo, N. T. Dintcheva, F. Giannici and F. D'Anna, Ionic liquids gels: Soft materials for

environmental remediation, *J. Colloid Interface Sci.*, 2018, **517**, 182–193.

40 I. A. Lawal, M. Klink, P. Ndungu and B. Moodley, Brief bibliometric analysis of "ionic liquid" applications and its review as a substitute for common adsorbent modifier for the adsorption of organic pollutants, *Environ. Res.*, 2019, **175**, 34–51.

41 B. Tang, J. Du, Q. Feng, J. Zhang, D. Wu, X. Jiang, Y. Dai and J. Zou, Enhanced generation of hydroxyl radicals on well-crystallized molybdenum trioxide/nano-graphite anode with sesame cake-like structure for degradation of bio-refractory antibiotic, *J. Colloid Interface Sci.*, 2018, **517**, 28–39.

42 T.-T. Zhu, Y.-B. Zhang, Y.-W. Liu and Z.-S. Zhao, Electrostimulation enhanced ammonium removal during Fe(III) reduction coupled with anaerobic ammonium oxidation (Feammox) process, *Sci. Total Environ.*, 2020, **751**, 141703.

43 Y. Pi, X. Feng, Y. Song, Z. Xu, Z. Li and W. Lin, Metal-Organic Frameworks Integrate Cu Photosensitizers and Secondary Building Unit-Supported Fe Catalysts for Photocatalytic Hydrogen Evolution, *J. Am. Chem. Soc.*, 2020, **142**, 10302–10307.

44 C. P. Tso, D. T. F. Kuo and Y. H. Shih, Removal of hexabromocyclododecane by carboxymethyl cellulose stabilized Fe and Ni/Fe bimetallic nanoparticles: The particle stability and reactivity in water, *Chemosphere*, 2020, **250**, 9.

45 X. Li, P. Liu, X. Niu, K. Ye, L. Ni, D. Du, J. Pan and Y. Lin, Tri-functional Fe-Zr bi-metal-organic frameworks enable high-performance phosphate ion ratiometric fluorescent detection, *Nanoscale*, 2020, **12**, 19383–19389.

46 J. Xu, J. Guo, M. Xu and X. Chen, Enhancement of microbial redox cycling of iron in zero-valent iron oxidation coupling with deca-brominated diphenyl ether removal, *Sci. Total Environ.*, 2020, **748**, 141328.

47 M. Saifuddin, J. Bae and K. S. Kim, Role of Fe, Na and Al in Fe-Zeolite-A for adsorption and desorption of phosphate from aqueous solution, *Water Res.*, 2019, **158**, 246–256.

48 K. Shehzad, M. Ahmad, C. Xie, D. Y. Zhan, W. Wang, Z. X. Li, W. H. Xu and J. H. Liu, Mesoporous zirconia nanostructures (MZN) for adsorption of As(III) and As(V) from aqueous solutions, *J. Hazard. Mater.*, 2019, **373**, 75–84.

49 Y. Wei, H. Liu, C. Liu, S. Luo, Y. Liu, X. Yu, J. Ma, K. Yin and H. Feng, Fast and efficient removal of As(III) from water by CuFe(2)O(4) with peroxymonosulfate: Effects of oxidation and adsorption, *Water Res.*, 2019, **150**, 182–190.